Probing QCD critical point and induced gravitational wave by black hole physics

Rong-Gen Cai[b,c], Song He[a,d], Li Li[b,c] and Yuan-Xu Wang[a]
[a] *Center for Theoretical Physics and College of Physics, Jilin University, Changchun 130012, People's Republic of China*
[b] *CAS Key Laboratory of Theoretical Physics, Institute of Theoretical Physics, Chinese Academy of Sciences, Beijing 100190, China*
[c] *School of Fundamental Physics and Mathematical Sciences, Hangzhou Institute for Advanced Study, UCAS, Hangzhou 310024, China and*
[d] *Max Planck Institute for Gravitational Physics (Albert Einstein Institute), Am Mühlenberg 1, 14476 Golm, Germany**
(Dated: January 7, 2022)

The Quantum Chromodynamics (QCD) phase diagram involves the behaviors of strongly interacting matter under extreme conditions and remains an important open problem. Based on the non-perturbative approach from the gauge/gravity duality, we construct a family of black holes that provide a dual description of the QCD phase diagram at finite chemical potential and temperature. The thermodynamic properties from the model are in good agreement with the state-of-the-art lattice simulations. We then predict the location of the critical endpoint and the first-order phase transition line. Moreover, we present the energy spectrum of the stochastic gravitational-wave background associated with the QCD first-order transition, which is found to be detected by IPTA and SKA, while by NANOGrav with less possibility.

Introduction– As one of the most interesting and fundamental challenges of high energy physics, the phase diagram of QCD has been under intensive investigation. It involves the behaviors of strongly interacting matter under extreme conditions [1–3], ranging from cosmology and astrophysics to heavy-iron collisions. Due to the difficulty of strong interaction in the non-perturbative regime, thus far, it has not been possible to obtain the full QCD phase diagram directly from QCD in terms of the temperature T and the baryon chemical potential μ_B or baryon number density ρ_B. While the lattice QCD can give reliable information from the first principle at zero density [4–6], it fails at finite density due to the famous sign problem [2]. Although the lattice data can be extended to finite μ_B via Taylor series expansion around $\mu_B = 0$ [7–9], such an approach can only be reliable at small μ_B. Meanwhile, many low energy effective models have been proposed to study the QCD phase diagram in certain conditions, such as [10–12]. Nevertheless, it is now well believed that QCD is in a confinement phase at low T and small μ_B, while it becomes deconfined at high T and large μ_B. Moreover, the transition from the confinement to the deconfinement phases is a crossover at small chemical potentials $\mu_B < \mu_C$ and becomes a first-order one for large $\mu_B > \mu_C$. Thus, there exists a critical endpoint (CEP) at which the first-order line ends up to the critical chemical potential μ_C.

On the other hand, the gauge/gravity duality [13–16] offers a powerful non-perturbative approach to solve the strongly coupled non-Abelian gauge theories by mapping to a weakly coupled gravity system with one higher dimension. In particular, it provides a convenient way to incorporate real-time dynamics and transport properties at finite temperature and density. The construction of the QCD phase diagram in such a holographic approach was initiated from [17–19], where the Einstein-Maxwell-dilaton (EMD) theory was used to mimic properties in the QCD phase diagram. Since then, several attempts have been made towards the phase diagram in the $T - \mu_B$ plane (see *e.g.* [20–28]). As the model parameters are fixed by matching to lattice QCD results, to make a reliable prediction at finite μ_B, it is crucial to use up-to-data lattice simulation. Moreover, in most studies [23, 24, 26, 27] thermodynamic variables were obtained by integrating the naive first law of thermodynamics of the hairy black hole for which its validity is still under investigation [29–32].

To solve these issues, in this letter we find a holographic QCD (hQCD) model in which all parameters are fixed using state-of-the-art lattice QCD data [6] at $\mu_B = 0$, generated by highly improved stagger fermion action. Moreover, all thermodynamic quantities are computed directly from holographic renormalization together with the so-called thermodynamic consistency relations. We then manage to make precise predictions for the QCD phase diagram at finite μ_B, in particular, a first-order line and a CEP located at $(T_C = 105\text{MeV}, \mu_C = 558\text{MeV})$. The thermodynamic quantities at small μ_B are in good agreement with the recent lattice QCD results [9]. Our model has three fewer parameters compared to the model in [27] which agreed with the old simulation data [5] and was claimed to be the simplest model in the current literature. The CEP is fixed both by the thermodynamics and the expectation value of the Polyakov loop operator which is an effective order parameter for the deconfinement transition in the unquenched QCD. Moreover, the strong first-order phase transition (SFOPT) in the early universe is a potentially important source for stochastic gravitational-wave (GW) background (see *e.g.* [33–36] and references therein).

While various scenarios of new physics beyond the standard model of particle physics were considered to engineer an SFOPT in the literature, our present model provides a scenario for phase transition GWs within the standard model. We find that the resulting GW signals can be detected *e.g.* by IPTA and SKA, while by NANOGrav with less possibility.

Holographic model –We begin with the five-dimensional EMD theory

$$S = \frac{1}{2\kappa_N^2}\int d^5x\sqrt{-g}\Big[\mathcal{R} - \frac{1}{2}\nabla_\mu\phi\nabla^\mu\phi - \frac{Z(\phi)}{4}F_{\mu\nu}F^{\mu\nu} - V(\phi)\Big]\,, \tag{1}$$

with the minimal set of fields for capturing the essential dynamics. Here κ_N^2 is the effective Newton constant. In addition to the metric $g_{\mu\nu}$ that characterizes the geometry, the real scalar ϕ (known as dilaton) encodes the running of the gauge coupling, and the Maxwell field A_μ accounts for a finite baryon density. $Z(\phi)$ and $V(\phi)$ are two phenomenological terms that will be fixed by matching to the lattice QCD at $\mu_B = 0$.

The hairy black hole reads

$$ds^2 = -f(r)e^{-\eta(r)}dt^2 + \frac{dr^2}{f(r)} + r^2 d\boldsymbol{x_3^2}\,, \qquad \phi = \phi(r), \quad A_t = A_t(r)\,, \tag{2}$$

where $d\boldsymbol{x_3^2} = dx^2 + dy^2 + dz^2$ and r is the holographic radial coordinate with the asymptotical anti-de Sitter (AdS) boundary at $r \to \infty$. Denoting the event horizon as r_h at which f vanishes, the temperature and entropy density can be obtained as

$$T = \frac{1}{4\pi}f'(r_h)e^{-\eta(r_h)/2}, \quad s = \frac{2\pi}{\kappa_N^2}r_h^3\,, \tag{3}$$

while the baryon chemical potential μ_B and density ρ_B can be obtained from A_t at the AdS boundary. We read off the energy density ϵ and pressure P directly by the dual stress-energy tensor via the holographic renormalization [37, 38]. We refer to the Appendix for more details. Then, the equation of state (EOS) and transport properties can be exactly determined. The form of V and Z is partially motivated by the one in [17–19], although the model of [17–19] was not able to simultaneously fit the lattice data for equilibrium and near-equilibrium features quantitatively. By global fitting the state-of-the-art lattice data [6, 9] with $(2+1)$-flavors at zero net-baryon density, the hQCD model can be fixed to be

$$\begin{aligned} V(\phi) &= -12\cosh[c_1\phi] + (6c_1^2 - \frac{3}{2})\phi^2 + c_2\phi^6\,,\\ \kappa_N^2 &= 2\pi(1.68), \quad \phi_s = 1085\text{MeV}\,,\\ Z(\phi) &= \frac{1}{1+c_3}\text{sech}[c_4\phi^3] + \frac{c_3}{1+c_3}e^{-c_5\phi}\,, \end{aligned} \tag{4}$$

with $c_1 = 0.7100, c_2 = 0.0037, c_3 = 1.935, c_4 = 0.085, c_5 = 30$. Here ϕ_s is the source term of the scalar field ϕ, which essentially breaks the conformal symmetry and plays the role of energy scale.

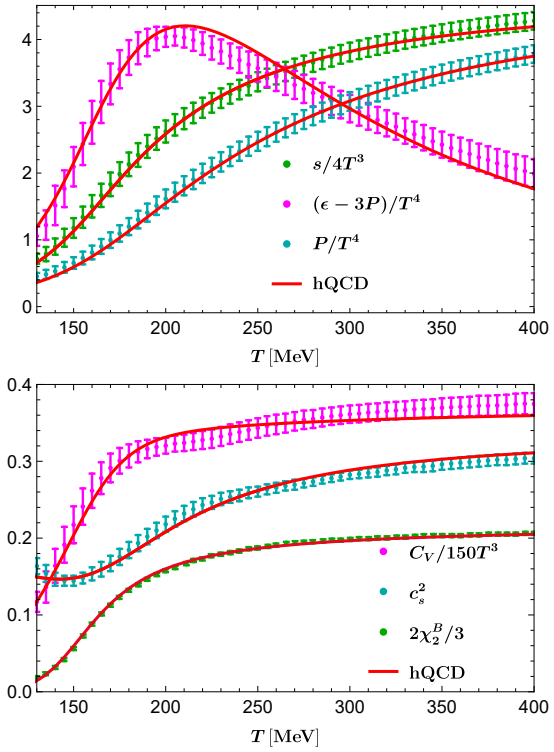

FIG. 1. Thermodynamics at $\mu_B = 0$. Data with error bars are from the latest lattice QCD [6, 9], while solid curves from our hQCD model, including entropy density s, trace anomaly $(\epsilon - 3P)$, pressure P, specific heat C_V, squared sound speed c_s^2 and baryon susceptibility.

The fitting results are presented in Fig. 1. In addition to the EOS (upper panel), the sound speed $c_s = \sqrt{(dP/d\epsilon)_{\mu_B}}$, the specific heat $C_V = (d\epsilon/dT)_{\mu_B}$, and the second-order baryon susceptibility $\chi_2^B = (d\rho_B/d\mu_B)_T$ at zero density, which are three important quantities characterizing QCD transition, agree with the lattice data quantitatively, see the lower panel of Fig. 1. We also compare the holographic results to the latest Taylor-expanded lattice QCD [9] in Fig. 2. One can see that the holographic predictions are in quantitative agreement with the lattice results that are available for small chemical potentials, which provides strong support for the hQCD model we consider. Moreover, our setup is much simpler than the one in [27] which was claimed to be the only effective holographic model that can simultaneously describe those thermodynamic variables at a quantitative level [39].

QCD phase diagram–After fixing the holographic model completely by matching the lattice simulations, we

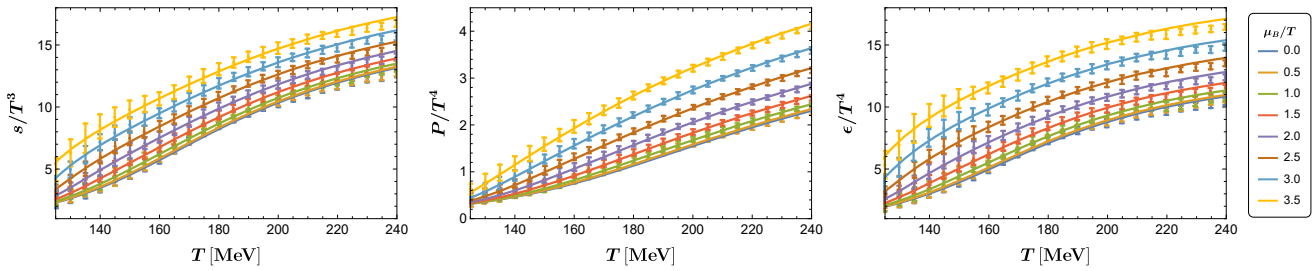

FIG. 2. s(left), P(center) and ϵ(right) at small chemical potentials. Our holographic computations (solid curves) are compared with the latest lattice QCD results from [9].

can now construct the phase diagram in the $T-\mu_B$ plane by solving numerically a set of black holes. We find that, as μ_B is increased, the crossover that takes place on the T-axis is sharpened into a first-order line at the CEP (see Fig. 3). Since the transition from $\mu_B = 0$ up to the CEP is a smooth crossover, there is no unique way to determine the transition temperature in the literature. Some good probes characterizing the drastic change of degrees of freedom between the quark gluon plasma (QGP) and the hadron gas are the minimum of c_s^2 and the maximally increasing point of χ_B^2. The transition lines from the two probes are shown in Fig. 3. The probing transition temperatures at zero μ_B compare well with lattice QCD predictions for the same up to the quark-hadron transition region around $140-160$MeV [40–42]. While they do not coincide quantitatively in the crossover region, they yield similar behavior and are of the same order of magnitude. Moreover, they do come together at the critical point μ_C.

For a baryon chemical potential above μ_C, the QCD transition becomes first-order, for which the transition point can be fixed uniquely by the free energy from the holographic computation (see the solid black line of Fig. 3). Note that the expectation value of Polyakov loop operator $\langle\mathcal{P}\rangle$ is a reasonable probe to the deconfinement phase transition (see Appendix for the computation of $\langle\mathcal{P}\rangle$). For a given $\mu_B > \mu_C$, we can obtain a range of T within which the first-order transition should happen (see the orange region of Fig. 3). It is manifest that the first order line determined by the free energy lies in the orange region, which may implies that the QCD transition from our hQCD model is associated with the deconfinement phase transition. The first order line decreases monotonically with μ_B. Although we are not able to see when the line will terminate, our numerics suggest that the transition temperature becomes significantly small, roughly, larger than $\mu_B \sim 1050$MeV beyond which no stable black holes have been found. In this region, there might be color superconductivity or related phenomena to set in.

The CEP predicted from our hQCD model is located at $(T_C = 105\text{MeV}, \mu_C = 558\text{MeV})$ (the red dot of Fig. 3). We also show the location of CEP from various models and note that the current best lattice estimation suggests that the CEP is likely above $\mu_B \sim 300$MeV [53, 54]. The variation in prior is considerable, but most of them are closed to the transition line we find. Moreover, compared with other predictions, our CEP is close to the ones obtained by Schwinger–Dyson equation [47, 48] and functional renormalization group [51] respectively. Nevertheless, all our predictions are at least qualitatively consistent with consensus expectations for the QCD phase diagram. Unfortunately, the CEP predicted from our theory is beyond the scope of some ongoing and future experiments, such as RHIC [55], FAIR [56, 57] and NICA [58]. Nevertheless, an important potential way to probe the phase diagram is from the GWs. Some preliminary studies on the GW spectra from holographic QCD were summarized in [59].

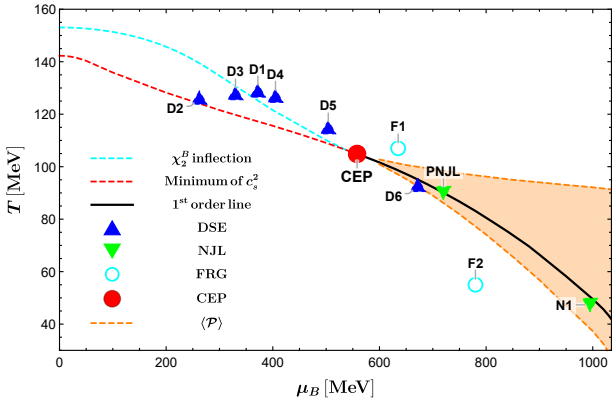

FIG. 3. The QCD phase diagram predicted from our model. The minimum of c_s^2 and the maximally increasing point of the χ_B^2 are denoted by dashed red and cyan lines, respectively. The first-order phase transition line (solid black line) is determined by free energy. The orange region comes from the Polyakov loop $\langle\mathcal{P}\rangle$. Our result for the location the CEP is $T_C = 105\text{MeV}, \mu_C = 558\text{MeV}$ (bold red dot). The CEP obtained by different approaches are presented as well, including Schwinger–Dyson equation (DSE), Nambu–Jona-Lasinio models (NJL), and Functional renormalization group (FRG). DSE: D1-D6 are from [43–48]. NJL: PNJL is from [49] and NJL1 from [50]. FRG: F1-F2 are from [51, 52].

GWs from QCD phase transition–To estimate the stochastic GWs from our hQCD model, we concentrate on the phase transition where bubbles of the broken phase nucleate and expand in the presence of a plasma of standard model particles. It has been argued that higher-order corrections prevent true runaway transitions from occurring [60], we will specialize in the case for which the bubble wall terminal velocity $v_w < 1$. For these non-runway bubbles, the GWs are dominated by sound waves with the energy spectrum [61]

$$h^2\Omega_{GW}(f) = 8.5\times10^{-6}\left(\frac{100}{g_n}\right)^{1/3}\left(\frac{\kappa\alpha}{1+\alpha}\right)^2 \times\left(\frac{H_n}{\beta}\right)v_w S_{SW}(f)\,. \tag{5}$$

Here α is the phase transition strength parameter and β/H_n the inverse time duration of the phase transition with H_n the Hubble rate at the nucleation temperature T_n. g_n describes the number of degrees of freedom at T_n and κ the fraction of the bulk kinetic energy in the plasma relative to the available vacuum energy. The spectral shape S_{SW} and the peak frequency f_{SW} are, respectively, given by

$$S_{SW}(f) = \left(\frac{f}{f_{SW}}\right)^3\left[\frac{7}{4+3(f/f_{SW})^2}\right]^{7/2},$$
$$f_{SW} = 1.9\times10^{-8}\left(\frac{\beta}{H_n}\right)\left(\frac{T_n}{100\,\text{Mev}}\right)\left(\frac{g_n}{100}\right)^{1/6}\text{Hz}\,. \tag{6}$$

We will fix g_* and v_w at their typical values with $g_* = 37$ [62] and $v_w = 0.95$ for which $\kappa = \frac{\alpha}{0.73+0.083\sqrt{\alpha}+\alpha}$. To account for the uncertainty in the duration β/H_n, we will scan the space with $4 < \beta/H_n < 80$. The last two crucial parameters can be read off from our model: T_n is approximately by the critical temperature of the first-order transition, and α is defined as the trace anomaly difference [34]

$$\alpha = \frac{4(\theta_+ - \theta_-)}{3w_+}\,, \tag{7}$$

between the false (+) and true (−) vacuums. Here $\theta = (\epsilon - 3P)/4$ is the trace anomaly and $w = \epsilon + P$ the enthalpy. In Fig. 4 we show the GW energy spectrum from the first-order transition for two representative values beyond CEP. We find that by increasing the chemical potential, the strength of the GW signal will increase, while the peak frequency will slightly decrease. The energy density of GWs produced from the first-order QCD phase transition can reach 10^{-9} around 10^{-8}Hz. While out of reach of LISA, it can be detected by IPTA and SKA. The detection from NANOGrav is possible for extreme scenarios with small values of $\beta/H_n \sim \mathcal{O}(1)$.

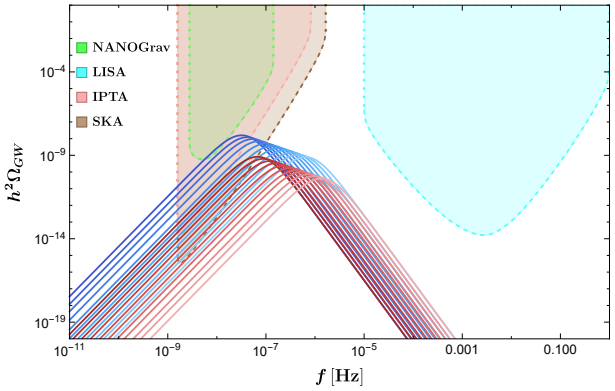

FIG. 4. Stochastic GW spectrum from the first order QCD phase transition predicted by our holographic model. Parameters extracted from the holographic model are $(\mu, T, \alpha) = (560\,\text{MeV}, 104.71\,\text{MeV}, 0.13)$ (red band) and $(1000\,\text{MeV}, 49.53\,\text{MeV}, 0.33)$ (blue band) with the variation of β/H_n. The upper curve in each band is for $\beta/H_n = 4$ and the lower curve is for $\beta/H_n = 80$. The sensitivity curves from [63] for four different experiments (NANOGrav, LISA, IPTA and SKA) are included.

Discussions–In this work, we build up a bottom-up holographic model to confront the most recent lattice results for EOS and offer a reliable first-order transition line and CEP in the QCD phase diagram. By computing thermodynamic quantities via holographic renormalization, the EOS is found to be quantitatively matched with the latest lattice QCD simulation. The QCD first-order transition line is fixed from the free energy and the corresponding CEP in the $T-\mu_B$ plane is predicted at $(T_C = 105\text{MeV}, \mu_C = 558\text{MeV})$. As a consistency check, we evaluate the expectation value of the Polyakov loop operator which yields the same CEP and suggests that the transition is closely associated with deconfinement. The GW energy spectrum from our hQCD model is within the projected sensitivity of IPTA and SKA, thus can be potentially detected in the near future.

Dedicating to a precise characterization of the properties and differences of the two phases along the first-order phase transition is an interesting direction for further study. In the current investigation, we have set up the preliminary hQCD model to quantitatively study the phase transition in the QCD phase diagram. The current model captures the characteristic confining properties and many other relevant physical quantities should be taken into account to complete the phase diagram, including the chiral condensation and the transport properties in QGP and hadron gas. In addition, the present results, in particular those regarding the CEP, should be embedded into the framework of a more general and multidimensional view of the QCD phase diagram, including an external magnetic field, an isospin chemical potential, and a rotation. It will be interesting

to consider the real-time dynamics in our hQCD model far-from-equilibrium.

Acknowledgements–We thank Heng-Tong Ding, Mei Huang, De-Fu Hou, Yi-Bo Yang, Danning Li, Zhibin Li, Shinya Matsuzaki, Shao-Jiang Wang, Yi Yang, Shou-Long Li and Peihung Yuan for stimulating discussions. This work is supported in part by the National Key Research and Development Program of China Grants No.2020YFC2201501 and No.2020YFC2201502, in part by the National Natural Science Foundation of China Grants No.12075101, No.12047569, N0.12122513, No.12075298, No.11991052 and No.12047503, in part by the Key Research Program of the Chinese Academy of Sciences (CAS) Grant NO. XDPB15 and by the CAS Project for Young Scientists in Basic Research YSBR-006. S.H. also would like to appreciate the financial support from Jilin University and Max Planck Partner group.

APPENDICES

Equations of motion– From the action (1) in the main text we can derive the equations of motion that are given as follows.

$$\begin{aligned}\nabla_\mu\nabla^\mu\phi-\frac{\partial_\phi Z}{4}F_{\mu\nu}F^{\mu\nu}-\partial_\phi V=0\,,\\ \nabla^\nu(ZF_{\nu\mu})=0\,,\\ \mathcal{R}_{\mu\nu}-\frac{1}{2}\mathcal{R}g_{\mu\nu}=\frac{1}{2}\partial_\mu\phi\partial_\nu\phi+\frac{Z}{2}F_{\mu\rho}F_\nu{}^\rho\\ +\frac{1}{2}\big(-\frac{1}{2}\nabla_\mu\phi\nabla^\mu\phi-\frac{Z}{4}F_{\mu\nu}F^{\mu\nu}-V\big)g_{\mu\nu}\,.\end{aligned}\tag{8}$$

As the dual system lives in a spatial plane, we choose the Poincaré coordinates with r the radial direction in the bulk. The metric ansatz reads

$$ds^2=-f(r)e^{-\eta(r)}dt^2+\frac{dr^2}{f(r)}+r^2(dx^2+dy^2+dz^2)\,,\tag{9}$$

together with

$$\phi=\phi(r),\quad A_t=A_t(r)\,.\tag{10}$$

We denote the event horizon as r_h at which f vanishes. Then the temperature and entropy density are given by

$$T=\frac{1}{4\pi}f'(r_h)e^{-\eta(r_h)/2},\quad s=\frac{2\pi}{\kappa_N^2}r_h^3\,.\tag{11}$$

Substituting the ansatz into (8), we obtain the following independent equations of motion.

$$\begin{aligned}\phi''+\left(\frac{f'}{f}-\frac{\eta'}{2}+\frac{3}{r}\right)\phi'+\frac{\partial_\phi Z}{2f}e^\eta A_t'^2-\frac{1}{f}\partial_\phi V=0\,,\\ \partial_r(e^{\eta/2}\,r^3\,ZA_t')=0\,,\\ \frac{\eta'}{r}+\frac{1}{3}\phi'^2=0\,,\\ \frac{2}{r}\frac{f'}{f}-\frac{\eta'}{r}+\frac{Z}{3f}e^\eta A_t'^2+\frac{2}{3f}V+\frac{4}{r^2}=0\,,\end{aligned}\tag{12}$$

where the prime denotes the derivative with respect to r. Both $Z(\phi)$ and $V(\phi)$ will be determined by matching to the lattice QCD at $\mu_B=0$.

In what follows we will specify these two functions as

$$\begin{aligned}V(\phi)&=-12\cosh[c_1\phi]+(6c_1^2-\frac{3}{2})\phi^2+c_2\phi^6\,,\\ Z(\phi)&=\frac{1}{1+c_3}\mathrm{sech}[c_4\phi^3]+\frac{c_3}{1+c_3}e^{-c_5\phi}\,,\end{aligned}\tag{13}$$

where c_1,c_2,c_3,c_4,c_5 are free parameters of the model. These model parameters capture the physical properties of realistic QCD,*e.g.* EOS and baryon susceptibility. Near the AdS boundary $r\to\infty$ where $\phi\to 0$, one has

$$\begin{aligned}Z(\phi)&=1+\mathcal{O}(\phi)\,,\\ V(\phi)&=-12-\frac{3}{2}\phi^2+\mathcal{O}(\phi^4)\,.\end{aligned}\tag{14}$$

Therefore, the cosmological constant is given by $\Lambda=-6$ (the AdS radius $L=1$). The scaling dimension of the dual scalar operator is $\Delta=3$ which is different from that in [17, 19, 23, 24, 27].

Boundary expansions– To obtain the numerical solutions for $f(r),\eta(r),\phi(r)$ and $A_t(r)$, we should specify suitable boundary conditions at both the event horizon r_h and the AdS boundary $r\to\infty$. The smoothness of the event horizon yields the following analytic expansion in terms of $(r-r_h)$ in the IR:

$$\begin{aligned}f&=f_h(r-r_h)+\dots\,,\\ \eta&=\eta_h^0+\eta_h^1(r-r_h)+\dots\,,\\ A_t&=a_h(r-r_h)+\dots\,,\\ \phi&=\phi_h^0+\phi_h^1(r-r_h)+\dots\,.\end{aligned}\tag{15}$$

After substituting (15) into the equations of motion (12), one finds four independents coefficients $(r_h,a_h,\eta_h^0,\phi_h^0)$. On the other hand, near the AdS boundary, we obtain

the following asymptotic expansion:

$$\begin{aligned}
\phi(r) &= \frac{\phi_s}{r} + \frac{\phi_v}{r^3} - \frac{\ln(r)}{6r^3}(1-6c_1^4)\phi_s^3 + \mathcal{O}(\frac{\ln(r)}{r^5})\,.\\
A_t(r) &= \mu_B - \frac{2\kappa_N^2\rho_B}{2r^2} - \frac{2\kappa_N^2\rho_B\, c_3\, c_5\, \phi_s}{3(1+c_3)\, r^3}\\
&\quad + \frac{2\kappa_N^2\rho_B\, \phi_s^2\, ((1+c_3)^2 - 6(-1+c_3)\, c_3\, c_5^2)}{48(1+c_3)^2\, r^4}\\
&\quad + \frac{2\kappa_N^2\rho_B\, c_3\, c_5\, (-10\, c_5^2\, (1+(-4+c_3)\, c_3))\, \phi_s^3}{300(1+c_3)^3\, r^5}\\
&\quad + \frac{2\kappa_N^2\rho_B\, c_3\, c_5\, \big((7-12\, c_1^4)\, \phi_s^3 - 60\ \phi_v\big)}{300(1+c_3)\, r^5}\\
&\quad - \frac{2\kappa_N^2\rho_B\, c_3\, c_5\, \phi_s^3(-1+6\, c_1^4)\ln(r)}{30(1+c_3)\, r^5} + \mathcal{O}(\frac{\ln(r)}{r^6})\,.\\
\eta(r) &= 0 + \frac{\phi_s^2}{6r^2} + \frac{(1-6c_1^4)\phi_s^4 + 72\phi_s\phi_v}{144r^4}\\
&\quad - \frac{\ln(r)}{12r^4}(1-6c_1^4)\phi_s^4 + \mathcal{O}(\frac{\ln(r)^2}{r^6})\,.\\
f(r) &= r^2\Big[1 + \frac{\phi_s^2}{6r^2} + \frac{f_v}{r^4} - \frac{\ln(r)}{12r^4}(1-6c_1^4)\phi_s^4\\
&\quad + \mathcal{O}\Big(\frac{\ln(r)^2}{r^6}\Big)\Big]\,.
\end{aligned} \tag{16}$$

Note that we have taken the normalization of the time coordinate at the boundary such that $\eta(r\to\infty)=0$. ϕ_s is the source of the scalar operator of the boundary theory, which essentially breaks the conformal symmetry and plays the role of the energy scale.

Before proceeding, we point out that the equations of motion (12) have two independent scaling symmetries:

$$t \to \lambda_t\, t\,,\quad e^\eta \to \lambda_t^2\, e^\eta\,,\quad A_t \to \lambda_t^{-1} A_t\,, \tag{17}$$

$$r \to \lambda_r\, r\,,\qquad f \to \lambda_r^2\, f\ ,\quad A_t \to \lambda_r\, A_t\,, \tag{18}$$

with λ_t and λ_r constants. Thus, we can first set $\eta_h^0 = 0$ and $r_h = 1$ for performing numerics. After obtaining the numerical solutions, we should use the first symmetry to satisfy the asymptotic condition $\eta(r\to\infty)=0$ and use the second one to fix the energy scale ϕ_s.

Thermodynamics–We now compute the free energy density Ω which is identified as the temperature T times the renormalized action in the Euclidean signature. Since we consider a stationary problem, the Euclidean action is related to the Minkowski one by a minus sign. Moreover, we should include the Gibbons-Hawking boundary term for a well-defined Dirichlet variational principle and a surface counterterm for removing divergence. Therefore, we have

$$-\,\Omega V = T(S+S_\partial)_{on-shell}\,, \tag{19}$$

with $V=\int dxdydz$ and $t\in[0,1/T]$.

We work in the grand canonical ensemble for which the baryon chemical potential is fixed. For the model (13) we are considering, following the the holographic renormalization [37, 38], the boundary terms take the form

$$\begin{aligned}
S_\partial &= \tfrac{1}{2\kappa_N^2}\int_{r\to\infty} dx^4\sqrt{-h}\Big[2K - 6 - \tfrac{1}{2}\phi^2\\
&\quad - \tfrac{6c_1^4-1}{12}\phi^4\ln[r] - b\,\phi^4 + \tfrac{1}{4}F_{\rho\lambda}F^{\rho\lambda}\ln[r]\Big]\,,
\end{aligned} \tag{20}$$

where $h_{\mu\nu}$ is the induced metric at the AdS boundary and $K_{\mu\nu}$ is the extrinsic curvature defined by the outward pointing normal vector to the boundary.

Employing the equations of motion (12) and the asymptotical expansion (16), we obtain

$$\begin{aligned}
\Omega &= \lim_{r\to\infty}\Bigg[2e^{-\eta/2}r^2 f - e^{-\eta/2}r^3\sqrt{f}\Big(2K-6\\
&\qquad - \frac{1}{2}\phi^2 - \frac{6c_1^4-1}{12}\phi^4\ln(r) - b\phi^4\Big)\Bigg]\,,\\
&= \frac{1}{2\kappa_N^2}\left(f_v - \phi_s\phi_v - \frac{3-48b-8c_1^4}{48}\phi_s^4\right)\,.
\end{aligned} \tag{21}$$

The energy-momentum tensor of the dual boundary theory reads

$$\begin{aligned}
T_{\mu\nu} &= \lim_{r\to\infty}\frac{2}{\sqrt{-\det g}}\frac{\delta(S+S_\partial)_{on-shell}}{\delta g^{\mu\nu}},\\
&= \frac{1}{2\kappa_N^2}\lim_{r\to\infty} r^2\Big[2(Kh_{\mu\nu} - K_{\mu\nu} - 3h_{\mu\nu})\\
&\quad - (\frac{1}{2}\phi^2 + \frac{6c_1^4-1}{12}\phi^4\ln[r] + b\,\phi^4)h_{\mu\nu}\\
&\quad - (F_{\mu\rho}F_\nu{}^\rho - \frac{1}{4}h_{\mu\nu}F_{\rho\lambda}F^{\rho\lambda})\ln[r]\Big]\,,
\end{aligned} \tag{22}$$

Substituting (16), we obtain

$$\begin{aligned}
\epsilon &:= T_{tt} = \frac{1}{2\kappa_N^2}\left(-3f_v + \phi_s\phi_v + \frac{1+48b}{48}\phi_s^4\right)\,,\\
P &:= T_{xx} = T_{yy} = T_{zz}\\
&= \frac{1}{2\kappa_N^2}\left(-f_v + \phi_s\phi_v + \frac{3-48b-8c_1^4}{48}\phi_s^4\right)\,,
\end{aligned} \tag{23}$$

with vanishing non-diagonal components. One immediately finds that $P=-\Omega$, which is expected from thermodynamics. The trace of the energy-momentum tensor is given by

$$\epsilon - 3P = \frac{1}{2\kappa_N^2}\left(2\phi_s\phi_v + \frac{1-24b-3c_1^4}{6}\phi_s^4\right)\,. \tag{24}$$

It is manifest that there is a trace anomaly in the presence of the source term ϕ_s that breaks the conformal symmetry.

By integrating the second equation of (12), one has

$$\frac{1}{2\kappa_N^2}e^{\eta/2}\, r^3\, Z A_t' = \rho_B\,, \tag{25}$$

where the constant ρ_B is nothing but the charge density that can be computed using the standard holographic dictionary. Another useful radially conserved quantity reads [64, 65]

$$\mathcal{Q} = \frac{1}{2\kappa_N^2} r^3 e^{\eta/2} \left[r^2 \left(\frac{f}{r^2} e^{-\eta} \right)' - Z A_t A_t' \right], \tag{26}$$

which connects horizon to boundary data. Evaluating at the horizon, we obtain

$$\mathcal{Q} = Ts, \tag{27}$$

and therefore $\mathcal{Q} = 0$ signals the extremity. On the other hand, evaluating $\mathcal{Q}$ at the AdS boundary, we find

$$\mathcal{Q} = \epsilon + P - \mu_B \rho_B \,. \tag{28}$$

Therefore, we immediately obtain the expected thermodynamical relation

$$\Omega = \epsilon - T s - \mu_B \rho_B = -P, \tag{29}$$

where Ω is the free energy density (21).

After obtaining above thermodynamic quantities, we can also compute some important transport coefficients, including the sound speed $C_s = \sqrt{(dP/d\epsilon)_{\mu_B}}$, the specific heat $C_V = (d\epsilon/dT)_{\mu_B}$, and the second order baryon susceptibility $\chi_2^B = (d\rho_B/d\mu_B)_T$. These properties are compared to the state-of-the-art lattice data [6, 9] with $(2+1)$-flavors at zero baryon density, from which all free parameters of our hQCD model can be fixed, see Eq. (4) and Figs. 1 and 2 in the main text. Moreover, the parameter b that appears in the boundary terms (20) is chosen to be $b = -0.27341$.

Before ending this section, we compare the thermodynamics of the holographic model [5] to the state-of-the-art lattice QCD data [6] used in the present work. This holographic model was constructed to mimic the QCD thermodynamic at a quantitative level. As can be seen from Fig. 5, the model of [5] fails to fit the new lattice data for the temperature above 280MeV.

Polyakov Loop–With the gravitational background (9), one can extract the expectation value of the Polyakov loop operator [66] in terms of the holographic dictionary. For simplicity, one makes the coordinate transformation $z = \frac{1}{r}$ and field redefinition $f(r) = \frac{F(z)}{z^2}, \eta(r) = \Sigma(z), \phi(r) = \Phi(z)$. The background (9) now becomes

$$\mathrm{d}s^2 = \frac{1}{z^2} \left[-F(z) e^{-\Sigma(z)} \mathrm{d}t^2 + \frac{\mathrm{d}z^2}{F(z)} + d\boldsymbol{x}_3^2 \right]. \tag{30}$$

The world-sheet action for the Polyakov loop [20, 67] in the string frame reads

$$S_{NG} = -\frac{1}{2\pi\alpha'} \int \mathrm{d}^2\xi \, e^{\sqrt{\frac{2}{3}}\Phi(z)} \sqrt{\det[g_{MN}(\partial_a X^M)(\partial_b X^N)]}\,, \tag{31}$$

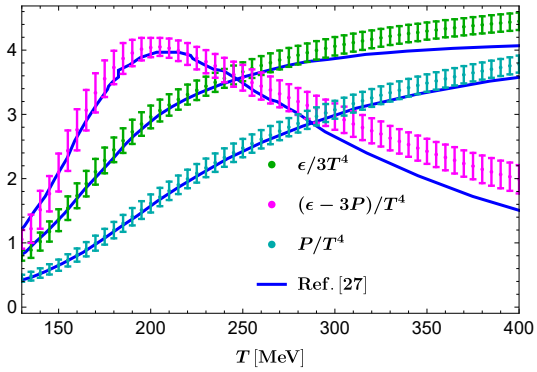

FIG. 5. Thermodynamics at $\mu_B = 0$. Data with error bars are from the latest Lattice QCD [6, 9], while blue curves from the holographic model of [27]. The entropy density ϵ, trace anomaly $(\epsilon - 3P)$ and pressure P fail to fit the lattice data for the temperature above 280MeV.

where g_{MN} is the target spacetime metric and g_{ab} is the induced metric. Here α' is the effective string tension.

Without loss of generality, we choose the static gauge condition $\xi^0 = t$, $\xi^1 = x$, $z = z(x)$, from which

$$g_{ab} = \begin{pmatrix} -\frac{F(z)e^{-\Sigma(z)}}{z^2} & 0 \\ 0 & \frac{1}{z^2}\left(\frac{z'(x)^2}{F(z)} + 1\right) \end{pmatrix}. \tag{32}$$

Thus, the action (31) becomes

$$\begin{aligned} S_{NG} &= -\frac{1}{2\pi\alpha'} \int \mathrm{d}t \int_{-\frac{\bar{r}}{2}}^{\frac{\bar{r}}{2}} \mathrm{d}x \frac{e^{\sqrt{\frac{2}{3}}\Phi(z) - \frac{\Sigma(z)}{2}}}{z^2} \sqrt{F(z) + z'(x)^2}\,, \\ &= -\frac{T}{\pi\alpha'} \int_{-\frac{\bar{r}}{2}}^{0} \mathrm{d}x \frac{e^{\sqrt{\frac{2}{3}}\Phi(z) - \frac{\Sigma(z)}{2}}}{z^2} \sqrt{F(z) + z'(x)^2}\,, \end{aligned} \tag{33}$$

with the boundary conditions

$$z(x=0) = z_0, \quad z'(x=0) = 0, \quad z(x = \pm\frac{\ell}{2}) = 0\,. \tag{34}$$

ℓ is the end point of the string on the boundary. The equation of motion is given by

$$\begin{aligned} &z'(x)^2 \\ =&F(z) \left(e^{-\Sigma(z) + \Sigma(z_0) + 2\sqrt{\frac{2}{3}}(\Phi(z) - \Phi(z_0))} (\frac{z_0}{z})^4 \frac{F(z)}{F(z_0)} - 1 \right). \end{aligned}$$

Plugging it into (33) and introducing the coordinate transformation $v = \frac{z}{z_0}$, we obtain

$$\begin{aligned} S_{NG} &= -\frac{T}{\pi\alpha'} \int_0^{z_0} \mathrm{d}z \frac{e^{\sqrt{\frac{2}{3}}\Phi(z) - \frac{\Sigma(z)}{2}}}{z'(x) z^2} \sqrt{F(z) + z'(x)^2}\,, \\ &= -\frac{T}{\pi\alpha' z_0} \int_0^1 \mathrm{d}v \frac{e^{-\frac{1}{2}\Sigma(v z_0) + \sqrt{\frac{2}{3}} v \Phi(v z_0)}}{v^2\, \tau(v)}\,, \end{aligned} \tag{35}$$

where $\tau(v)$ is

$$\tau(v) = \sqrt{1 - \frac{e^{-\Sigma(z_0)+\Sigma(vz_0)-2\sqrt{\frac{2}{3}}(-\Phi(z_0)+v\Phi(vz_0))}v^4 F(z_0)}{F(vz_0)}}\,.$$

The on-shell renormalized free energy for the Polyakov loop operator is given by

$$\langle \mathcal{P} \rangle = \frac{1}{\pi\alpha' z_0}\left[-1 + \int_0^1 \frac{\mathrm{d}v}{v^2}\left(\frac{e^{-\frac{1}{2}\Sigma(vz_0)+\sqrt{\frac{2}{3}}v\Phi(vz_0)}}{\tau(v)} - 1\right)\right]. \tag{36}$$

We then apply (36) to compute the expectation value of the Polyakov loop and to check whether the phase transition indicated by the free energy Ω is related to confinement/deconfinement. As shown in the upper panel of Fig. 6, once μ_B is gradually close to the critical endpoint μ_C, the swallowtails of free energy become smaller. Closing to μ_C, the swallowtails of the free energy and the region defined by the Polyakov loop shrink to the same point simultaneously. In the lower panel of Fig. 6, $\langle \mathcal{P} \rangle$ has a multiple value behavior with respect to the temperature, once the chemical potential crosses the critical value μ_C. There is no first principle to tell us where the precise transition point is in terms of $\langle \mathcal{P} \rangle$. Nevertheless, it gives us a range between maximal and minimal temperatures. The transition line obtained by the free energy Ω indeed lies in such region marked by the orange color in Fig. 3. Thus, the CEP and the first-order transition line may be associated with the confinement/deconfinement phase transition.

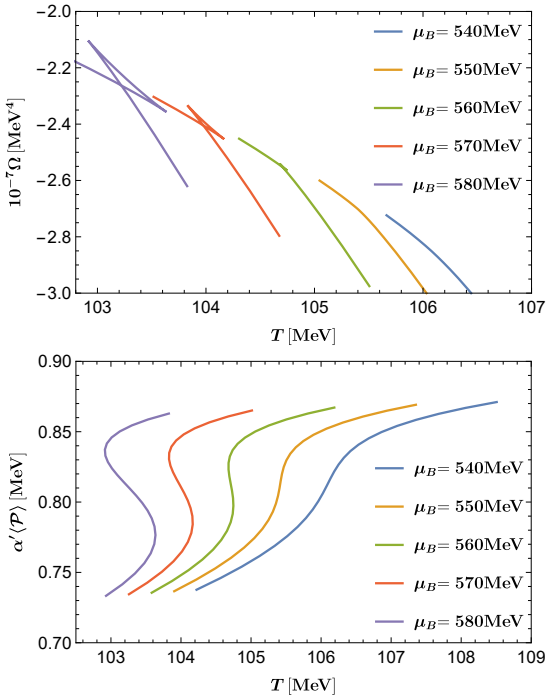

FIG. 6. Free energy Ω and $\langle \mathcal{P} \rangle$ for different values of μ_B. From right to left, μ_B increases. For $\mu > \mu_C$, free energy Ω and $\langle \mathcal{P} \rangle$ are multivalue functions of temperature, which implies that there exists a first order phase transition.

* cairg@itp.ac.cn,
hesong@jlu.edu.cn (corresponding author),
liliphy@itp.ac.cn (corresponding author),
yuanxu20@mails.jlu.edu.cn

[1] P. Braun-Munzinger and J. Wambach, "The Phase Diagram of Strongly-Interacting Matter," Rev. Mod. Phys. **81** (2009), 1031-1050 [arXiv:0801.4256 [hep-ph]].
[2] O. Philipsen, "The QCD equation of state from the lattice," Prog. Part. Nucl. Phys. **70** (2013), 55-107 [arXiv:1207.5999 [hep-lat]].
[3] S. Gupta, X. Luo, B. Mohanty, H. G. Ritter and N. Xu, "Scale for the Phase Diagram of Quantum Chromodynamics," Science **332** (2011), 1525-1528 [arXiv:1105.3934 [hep-ph]].
[4] S. Borsanyi, G. Endrodi, Z. Fodor, A. Jakovac, S. D. Katz, S. Krieg, C. Ratti and K. K. Szabo, "The QCD equation of state with dynamical quarks," JHEP **11** (2010), 077 [arXiv:1007.2580 [hep-lat]].
[5] S. Borsanyi, Z. Fodor, C. Hoelbling, S. D. Katz, S. Krieg and K. K. Szabo, "Full result for the QCD equation of state with 2+1 flavors," Phys. Lett. B **730** (2014), 99-104 [arXiv:1309.5258 [hep-lat]].
[6] A. Bazavov *et al.* [HotQCD], "Equation of state in (2+1)-flavor QCD," Phys. Rev. D **90** (2014), 094503 [arXiv:1407.6387 [hep-lat]].
[7] C. R. Allton, S. Ejiri, S. J. Hands, O. Kaczmarek, F. Karsch, E. Laermann, C. Schmidt and L. Scorzato, "The QCD thermal phase transition in the presence of a small chemical potential," Phys. Rev. D **66** (2002), 074507 [arXiv:hep-lat/0204010 [hep-lat]].
[8] D. Everett *et al.* [JETSCAPE], "Phenomenological constraints on the transport properties of QCD matter with data-driven model averaging," Phys. Rev. Lett. **126** (2021) no.24, 242301 [arXiv:2010.03928 [hep-ph]].
[9] S. Borsányi, Z. Fodor, J. N. Guenther, R. Kara, S. D. Katz, P. Parotto, A. Pásztor, C. Ratti and K. K. Szabó, "Lattice QCD equation of state at finite chemical potential from an alternative expansion scheme," Phys. Rev. Lett. **126** (2021) no.23, 232001 [arXiv:2102.06660 [hep-lat]].
[10] P. Braun-Munzinger, V. Koch, T. Schäfer and J. Stachel, "Properties of hot and dense matter from relativistic heavy ion collisions," Phys. Rept. **621** (2016), 76-126 [arXiv:1510.00442 [nucl-th]].
[11] M. A. Stephanov, "QCD phase diagram and the critical point," Prog. Theor. Phys. Suppl. **153** (2004), 139-156 [arXiv:hep-ph/0402115 [hep-ph]].
[12] K. Fukushima and C. Sasaki, "The phase diagram of nuclear and quark matter at high baryon density," Prog. Part. Nucl. Phys. **72** (2013), 99-154 [arXiv:1301.6377 [hep-ph]].
[13] J. M. Maldacena, "The Large N limit of superconformal field theories and supergravity," Adv. Theor. Math. Phys.

2 (1998), 231-252 [arXiv:hep-th/9711200 [hep-th]].

[14] S. S. Gubser, I. R. Klebanov and A. M. Polyakov, "Gauge theory correlators from noncritical string theory," Phys. Lett. B **428** (1998), 105-114 [arXiv:hep-th/9802109 [hep-th]].

[15] E. Witten, "Anti-de Sitter space and holography," Adv. Theor. Math. Phys. **2** (1998), 253-291 [arXiv:hep-th/9802150 [hep-th]].

[16] E. Witten, "Anti-de Sitter space, thermal phase transition, and confinement in gauge theories," Adv. Theor. Math. Phys. **2** (1998), 505-532 [arXiv:hep-th/9803131 [hep-th]].

[17] S. S. Gubser, A. Nellore, S. S. Pufu and F. D. Rocha, "Thermodynamics and bulk viscosity of approximate black hole duals to finite temperature quantum chromodynamics," Phys. Rev. Lett. **101** (2008), 131601 [arXiv:0804.1950 [hep-th]].

[18] O. DeWolfe, S. S. Gubser and C. Rosen, "A holographic critical point," Phys. Rev. D **83** (2011), 086005 [arXiv:1012.1864 [hep-th]].

[19] O. DeWolfe, S. S. Gubser and C. Rosen, "Dynamic critical phenomena at a holographic critical point," Phys. Rev. D **84** (2011), 126014 [arXiv:1108.2029 [hep-th]].

[20] R. G. Cai, S. He and D. Li, "A hQCD model and its phase diagram in Einstein-Maxwell-Dilaton system," JHEP **03** (2012), 033 [arXiv:1201.0820 [hep-th]].

[21] S. He, S. Y. Wu, Y. Yang and P. H. Yuan, "Phase Structure in a Dynamical Soft-Wall Holographic QCD Model," JHEP **04** (2013), 093 [arXiv:1301.0385 [hep-th]].

[22] T. Alho, M. Järvinen, K. Kajantie, E. Kiritsis, C. Rosen and K. Tuominen, "A holographic model for QCD in the Veneziano limit at finite temperature and density," JHEP **04** (2014), 124 [erratum: JHEP **02** (2015), 033] [arXiv:1312.5199 [hep-ph]].

[23] J. Knaute, R. Yaresko and B. Kämpfer, "Holographic QCD phase diagram with critical point from Einstein–Maxwell-dilaton dynamics," Phys. Lett. B **778** (2018), 419-425 [arXiv:1702.06731 [hep-ph]].

[24] R. Critelli, J. Noronha, J. Noronha-Hostler, I. Portillo, C. Ratti and R. Rougemont, "Critical point in the phase diagram of primordial quark-gluon matter from black hole physics," Phys. Rev. D **96** (2017) no.9, 096026 [arXiv:1706.00455 [nucl-th]].

[25] U. Gursoy, M. Jarvinen and G. Nijs, "Holographic QCD in the Veneziano Limit at a Finite Magnetic Field and Chemical Potential," Phys. Rev. Lett. **120** (2018) no.24, 242002 [arXiv:1707.00872 [hep-th]].

[26] Y. Yang and P. H. Yuan, 'QCD Phase Diagram by Holography," [arXiv:2011.11941 [hep-th]].

[27] J. Grefa, J. Noronha, J. Noronha-Hostler, I. Portillo, C. Ratti and R. Rougemont, "Hot and dense quark-gluon plasma thermodynamics from holographic black holes," Phys. Rev. D **104** (2021) no.3, 034002 [arXiv:2102.12042 [nucl-th]].

[28] T. Demircik, C. Ecker and M. Järvinen, "Dense and Hot QCD at Strong Coupling," [arXiv:2112.12157 [hep-ph]].

[29] L. Li, "On Thermodynamics of AdS Black Holes with Scalar Hair," Phys. Lett. B **815** (2021), 136123 [arXiv:2008.05597 [gr-qc]].

[30] T. Hertog and G. T. Horowitz, "Designer gravity and field theory effective potentials," Phys. Rev. Lett. **94**, 221301 (2005) [arXiv:hep-th/0412169 [hep-th]].

[31] A. Anabalon, D. Astefanesei, D. Choque and C. Martinez, "Trace Anomaly and Counterterms in Designer Gravity," JHEP **03**, 117 (2016) [arXiv:1511.08759 [hep-th]].

[32] H. Lu, C. N. Pope and Q. Wen, "Thermodynamics of AdS Black Holes in Einstein-Scalar Gravity," JHEP **03**, 165 (2015) [arXiv:1408.1514 [hep-th]].

[33] R. G. Cai, Z. Cao, Z. K. Guo, S. J. Wang and T. Yang, "The Gravitational-Wave Physics," Natl. Sci. Rev. **4** (2017) no.5, 687-706 [arXiv:1703.00187 [gr-qc]].

[34] C. Caprini, M. Chala, G. C. Dorsch, M. Hindmarsh, S. J. Huber, T. Konstandin, J. Kozaczuk, G. Nardini, J. M. No and K. Rummukainen, *et al.* "Detecting gravitational waves from cosmological phase transitions with LISA: an update," JCAP **03**, 024 (2020) [arXiv:1910.13125 [astro-ph.CO]].

[35] M. B. Hindmarsh, M. Lüben, J. Lumma and M. Pauly, "Phase transitions in the early universe," SciPost Phys. Lect. Notes **24**, 1 (2021) [arXiv:2008.09136 [astro-ph.CO]].

[36] L. Bian, R. G. Cai, S. Cao, Z. Cao, H. Gao, Z. K. Guo, K. Lee, D. Li, J. Liu and Y. Lu, *et al.* "The Gravitational-Wave Physics II: Progress," Sci. China Phys. Mech. Astron. **64** (2021), 120401 [arXiv:2106.10235 [gr-qc]].

[37] K. Skenderis, "Lecture notes on holographic renormalization," Class. Quant. Grav. **19** (2002), 5849-5876 [arXiv:hep-th/0209067 [hep-th]].

[38] S. de Haro, S. N. Solodukhin and K. Skenderis, "Holographic reconstruction of space-time and renormalization in the AdS / CFT correspondence," Commun. Math. Phys. **217** (2001), 595-622 [arXiv:hep-th/0002230 [hep-th]].

[39] As is shown in Appendix, this model [27] is not able to fit the new lattice data [6].

[40] A. Bazavov, T. Bhattacharya, M. Cheng, N. H. Christ, C. DeTar, S. Ejiri, S. Gottlieb, R. Gupta, U. M. Heller and K. Huebner, *et al.* "Equation of state and QCD transition at finite temperature," Phys. Rev. D **80** (2009), 014504 [arXiv:0903.4379 [hep-lat]].

[41] S. Borsanyi *et al.* [Wuppertal-Budapest], "Is there still any T_c mystery in lattice QCD? Results with physical masses in the continuum limit III," JHEP **09** (2010), 073 [arXiv:1005.3508 [hep-lat]].

[42] S. Borsanyi, Z. Fodor, S. D. Katz, S. Krieg, C. Ratti and K. Szabo, "Fluctuations of conserved charges at finite temperature from lattice QCD," JHEP **01** (2012), 138 [arXiv:1112.4416 [hep-lat]].

[43] X. y. Xin, S. x. Qin and Y. x. Liu, "Quark number fluctuations at finite temperature and finite chemical potential via the Dyson-Schwinger equation approach," Phys. Rev. D **90** (2014) no.7, 076006 [arXiv:2109.09935 [hep-ph]].

[44] F. Gao and Y. x. Liu, "QCD phase transitions via a refined truncation of Dyson-Schwinger equations," Phys. Rev. D **94** (2016) no.7, 076009 [arXiv:1607.01675 [hep-ph]].

[45] S. x. Qin, L. Chang, H. Chen, Y. x. Liu and C. D. Roberts, "Phase diagram and critical endpoint for strongly-interacting quarks," Phys. Rev. Lett. **106** (2011), 172301 [arXiv:1011.2876 [nucl-th]].

[46] C. Shi, Y. L. Wang, Y. Jiang, Z. F. Cui and H. S. Zong, "Locate QCD Critical End Point in a Continuum Model Study," JHEP **07** (2014), 014 [arXiv:1403.3797 [hep-ph]].

[47] C. S. Fischer, J. Luecker and C. A. Welzbacher, "Phase structure of three and four flavor QCD," Phys. Rev. D **90** (2014) no.3, 034022 [arXiv:1405.4762 [hep-ph]].

[48] F. Gao and J. M. Pawlowski, "QCD phase structure

from functional methods," Phys. Rev. D **102** (2020) no.3, 034027 [arXiv:2002.07500 [hep-ph]].

[49] Z. Li, K. Xu, X. Wang and M. Huang, "The kurtosis of net baryon number fluctuations from a realistic Polyakov–Nambu–Jona-Lasinio model along the experimental freeze-out line," Eur. Phys. J. C **79** (2019) no.3, 245 [arXiv:1801.09215 [hep-ph]].

[50] M. Asakawa and K. Yazaki, "Chiral Restoration at Finite Density and Temperature," Nucl. Phys. A **504** (1989), 668-684

[51] W. j. Fu, J. M. Pawlowski and F. Rennecke, "QCD phase structure at finite temperature and density," Phys. Rev. D **101** (2020) no.5, 054032 [arXiv:1909.02991 [hep-ph]].

[52] H. Zhang, D. Hou, T. Kojo and B. Qin, "Functional renormalization group study of the quark-meson model with ω meson," Phys. Rev. D **96** (2017) no.11, 114029 [arXiv:1709.05654 [hep-ph]].

[53] M. A. Stephanov, K. Rajagopal and E. V. Shuryak, "Event-by-event fluctuations in heavy ion collisions and the QCD critical point," Phys. Rev. D **60** (1999), 114028 [arXiv:hep-ph/9903292 [hep-ph]].

[54] A. Bazavov, H. T. Ding, P. Hegde, O. Kaczmarek, F. Karsch, E. Laermann, Y. Maezawa, S. Mukherjee, H. Ohno and P. Petreczky, *et al.* "The QCD Equation of State to $\mathcal{O}(\mu_B^6)$ from Lattice QCD," Phys. Rev. D **95** (2017) no.5, 054504 [arXiv:1701.04325 [hep-lat]].

[55] J. Adam *et al.* [STAR], "Nonmonotonic Energy Dependence of Net-Proton Number Fluctuations," Phys. Rev. Lett. **126** (2021) no.9, 092301 [arXiv:2001.02852 [nucl-ex]].

[56] T. Ablyazimov *et al.* [CBM], "Challenges in QCD matter physics –The scientific programme of the Compressed Baryonic Matter experiment at FAIR," Eur. Phys. J. A **53** (2017) no.3, 60 [arXiv:1607.01487 [nucl-ex]].

[57] M. Durante, P. Indelicato, B. Jonson, V. Koch, K. Langanke, U. G. Meißner, E. Nappi, T. Nilsson, T. Stöhlker and E. Widmann, *et al.* "All the fun of the FAIR: fundamental physics at the facility for antiproton and ion research," Phys. Scripta **94** (2019) no.3, 033001 [arXiv:1903.05693 [nucl-th]].

[58] A. N. Sissakian *et al.* [NICA], "The nuclotron-based ion collider facility (NICA) at JINR: New prospects for heavy ion collisions and spin physics," J. Phys. G **36** (2009), 064069

[59] S. L. Li, L. Shao, P. Wu and H. Yu, "NANOGrav signal from first-order confinement-deconfinement phase transition in different QCD-matter scenarios," Phys. Rev. D **104**, no.4, 043510 (2021) [arXiv:2101.08012 [astro-ph.CO]].

[60] D. Bodeker and G. D. Moore, "Electroweak Bubble Wall Speed Limit," JCAP **05**, 025 (2017) [arXiv:1703.08215 [hep-ph]].

[61] H. K. Guo, K. Sinha, D. Vagie and G. White, "The benefits of diligence: how precise are predicted gravitational wave spectra in models with phase transitions?," JHEP **06**, 164 (2021) [arXiv:2103.06933 [hep-ph]].

[62] More precisely, we take into account 8 gluons with 2 helicity states, 2 quarks, 2 antiquarks, each with 2 helicity states and 3 colors. Thus $c_2 = 2{\times}2{\times}2{\times}3{\times}7/8{+}2{\times}8 = 37$ with the factor 7/8 the usual fermionic statistic factor.

[63] K. Schmitz, "New Sensitivity Curves for Gravitational-Wave Signals from Cosmological Phase Transitions," JHEP **01**, 097 (2021) [arXiv:2002.04615 [hep-ph]].

[64] E. Kiritsis and L. Li, "Holographic Competition of Phases and Superconductivity," JHEP **01**, 147 (2016) [arXiv:1510.00020 [cond-mat.str-el]].

[65] R. G. Cai, L. Li and R. Q. Yang, "No Inner-Horizon Theorem for Black Holes with Charged Scalar Hairs," JHEP **03** (2021), 263 [arXiv:2009.05520 [gr-qc]].

[66] A. M. Polyakov, "String theory and quark confinement," Nucl. Phys. B Proc. Suppl. **68** (1998), 1-8 [arXiv:hep-th/9711002 [hep-th]].

[67] D. Li, S. He, M. Huang and Q. S. Yan, "Thermodynamics of deformed AdS_5 model with a positive/negative quadratic correction in graviton-dilaton system," JHEP **09** (2011), 041 [arXiv:1103.5389 [hep-th]].